Earth and Planetary Science Letters 300 (2010) 46–54

Contents lists available at ScienceDirect

Earth and Planetary Science Letters

journal homepage: www.elsevier.com/locate/epsl

Three thousand years of extreme rainfall events recorded in stalagmites from Spring Valley Caverns, Minnesota

Sushmita Dasgupta [a,b,*], Martin O. Saar [b], R. Lawrence Edwards [b], Chuan-Chou Shen [c], Hai Cheng [d,b], E. Calvin Alexander Jr. [b]

[a] Schlumberger, 1325 S Dairy Ashford Road, Houston TX 77077, USA
[b] Department of Geology and Geophysics, University of Minnesota, Minneapolis, MN 55455, USA
[c] High-Precision Mass Spectrometry and Environment Change Laboratory (HISPEC), Department of Geosciences, National Taiwan University, No. 1, Sec. 4, Roosevelt Rd., Taipei 106, Taiwan ROC
[d] Institute of Global Environmental Change, Xi'an Jiaotong, University, Xi'an, 710049, China

ARTICLE INFO

Article history:
Received 3 June 2010
Received in revised form 20 September 2010
Accepted 21 September 2010

Editor: P. DeMenocal

Keywords:
stalagmites
fluorescent bands
cave flooding
extreme rainfall events
confocal microscopy
paleoclimate

ABSTRACT

Annual layer analysis in two stalagmites collected from Spring Valley Caverns, southeastern Minnesota, reveals hydrological response of the cave to extreme rainfall events in the Midwest, USA. Cave-flooding events are identified within the two samples by the presence of detrital layers composed of clay sized particles. Comparison with instrumental records of precipitation demonstrates a strong correlation between these cave-flood events and extreme rainfall observed in the Upper Mississippi Valley. A simple model is developed to assess the nature of rainfall capable of flooding the cave. The model is first calibrated to the last 50-yr (1950–1998 A.D.) instrumental record of daily precipitation data for the town of Spring Valley and verified with the first 50 yr of record from 1900 to 1949 A.D. Frequency analysis shows that these extreme flood events have increased from the last half of the nineteenth century. Comparison with other paleohydrological records shows increased occurrence of extreme rain events during periods of higher moisture availability. Our study implies that increased moisture availability in the Midwestern region, due to rise in temperature from global warming could lead to an increase in the occurrence of extreme rainfall events.

1. Introduction

Studying past climate changes is critical to improve our understanding of past climate variability as well as predictions of future climate change. The latter requires a sound knowledge of the interrelationships between various climate parameters such as temperature and moisture variability. Furthermore, in the context of present-day global warming scenarios, we need to understand how changes in one climatic factor affect other climate parameters and how these parameters combine to determine the overall climatic outcome.

Climate change is characterized both by continuous variables such as temperature and humidity and by the frequency and magnitude of extreme, discontinuous variables, such as thunderstorms, hurricanes, and floods. As these extreme events can also be major modifiers of land surface, biosphere, and society, it is necessary to understand how climate change modifies the frequency and magnitude of extreme events. However, extreme events are not always registered by proxies, which typically record average parameter values. As a result, it is difficult to deduce past changes in extreme event frequency from such proxy data. For example, flood or hurricane frequencies, and changes thereof over time, are more difficult to estimate than temporal variations in temperature or rainfall.

Several studies have investigated modern extreme events in the U.S. (Karl et al., 1995; Kunkel and Andsager, 1999; Schumacher and Johnson, 2006; Yiou and Nogaj, 2004) addressing important questions including 1) how do these events vary through time and 2) what controls their frequency of occurrence. While difficult and often incomplete, it is also possible to examine past trends of extreme events to answer similar questions. For example, records of past hurricanes (Nyberg et al., 2007) and cyclones (Frappier et al., 2007) have been reconstructed in coastal regions. However, no dataset appears to exist for extreme rainfall events or thunderstorms in the mid-continental U.S. before the advent of instrumental records approximately one hundred years ago. To bridge this gap in climate record reconstructions, we focus on determining extreme rainfall events, henceforth referred to as extreme events, from geologic records of cave-flood occurrences.

Dorale et al. (2005) investigated detrital layers in thin sections of stalagmites collected from Crevice Cave, Missouri, and suggested that these layers represent cave-flood events. We build on this approach and further suggest that cave floods indicated by such detrital records in the stalagmites represent extreme rainfall events near the cave over the past 3000 yr. It is worth noting here that previous works on annual

* Corresponding author. Schlumberger, 1325 S Dairy Ashford Road, Houston TX 77077, USA. Tel.: +1 281 285 1502; fax: +1 281 285 1537.
E-mail address: sdasgupta3@slb.com (S. Dasgupta).

0012-821X/$ – see front matter © 2010 Elsevier B.V. All rights reserved.
doi:10.1016/j.epsl.2010.09.032

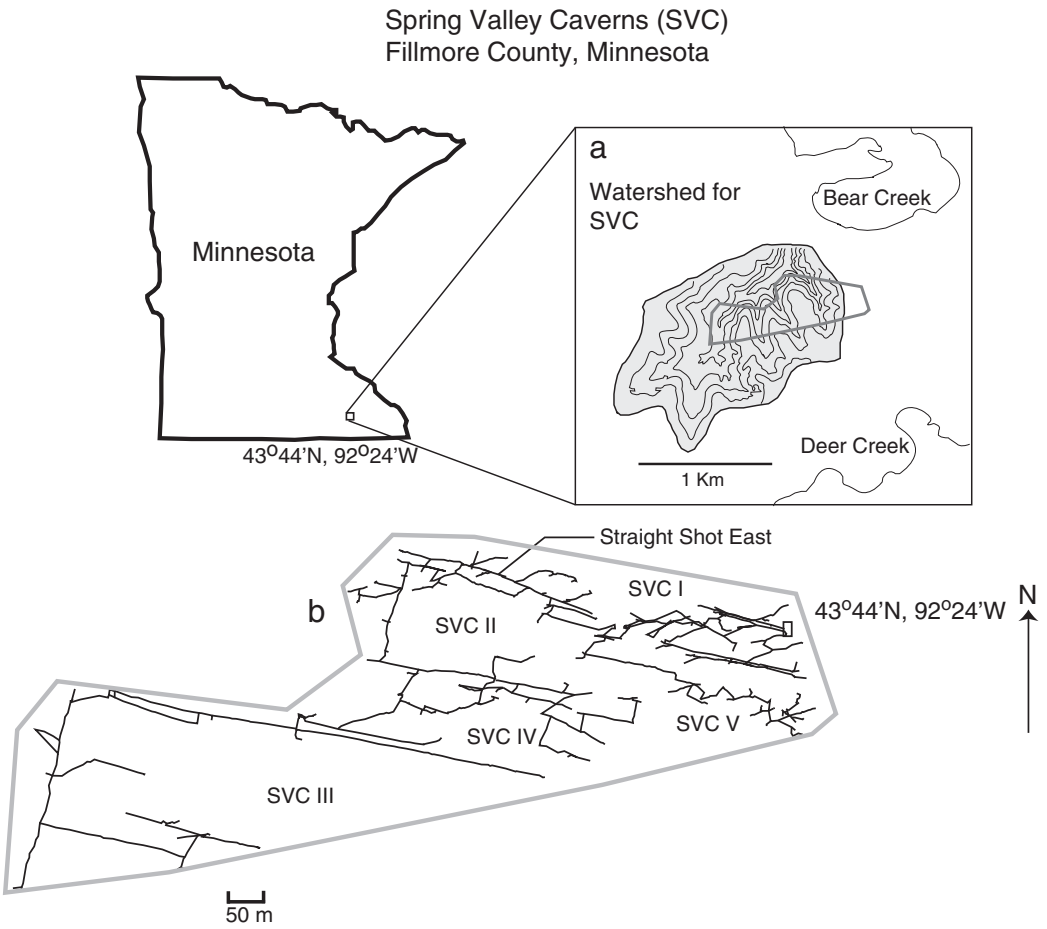

Fig. 1. a) Map showing the location of Spring Valley Caverns and its watershed between two streams, Bear Creek and Deer Creek. The shaded area marks the watershed corresponding to the cave. Contour intervals within the watershed are marked at every 10 ft (3.05 m). The solid gray line outlines the location of the cave. b) Detail map of Spring Valley Caverns (SVC) showing the five different sections of the cave. Latitude and longitude are given for the entrance to SVC I, marked by the rectangular box. This map was adopted after the original survey by David Gerboth (Minnesota Speleological Survey, 1995).

luminescent banding in stalagmites have focused on extracting climatological information from the banding themselves (e.g., Baker et al., 1998; Polyak and Asmerom, 2001). This present work utilizes the annual banding exclusively for the purpose of precise dating and cross checking between samples but fluorescent banding properties are not interpreted.

We study two stalagmites collected from Spring Valley Caverns in southeastern Minnesota (Fig. 1). Confocal fluorescence microscopy and electron microprobe analysis are used to image the samples' fluorescent bands and to determine their detrital compositions, respectively. The method of fluorescence imaging of the stalagmites was adopted and modified after the method of Luis A. Gonzalez (personal communication). The age of stalagmite layers is determined by both ^{230}Th dating and fluorescent band counting (Baker et al., 1993). Combining instrumental weather records with our observed data, we develop a simple hydrological model to simulate cave flooding, which suggests a relationship between cave floods and extreme rainfall events. Finally, we reconstruct the frequency of cave-flood occurrences and related extreme rainfall events per century revealing their trends over the last 3000 yr. The trends suggest an increase in extreme rainfall events during the latter half of the 19th century, coinciding with global warming trends.

2. Site and sample description

Two samples were collected from Spring Valley Caverns (SVC) (43°44′24″N, 92°24′36″W) situated in Fillmore county, (southeastern Minnesota, USA), about 6.4 km northwest of the town of Spring Valley. The cave is located in the Root River watershed of the Upper Mississippi Valley between Bear Creek in the north and Deer Creek in the south (Fig. 1), consisting of five interconnected divisions with a total length of approximately 8.7 km. The water flow direction in the cave is from southwest to northeast, as determined by mapping and dye traces.

We determined the watershed area of the cave system from the USGS topographic sheet for Spring Valley, MN (N4337.5–W9222.5/7.5). The area above the cave constitutes predominantly farmland that was formerly part of a hardwood oak forest.

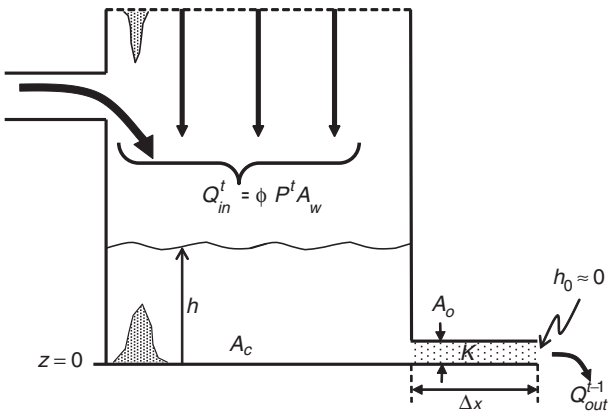

Fig. 2. Conceptual diagram approximating the cave as a tank with vertical walls. Q_{in} = flux of water into the cave; Φ = percentage infiltration; P_t = rate of rainfall; A_w = watershed area; A_c = cave area; A_o = outlet area; Q_{out} = flux of water out of the cave; t = time step; h = water level height; z = base level; Δx = horizontal length of the outlet; and K = hydraulic conductivity.

The modern data of temperature and precipitation in the region were obtained from the nearby town of Spring Valley. The town's instrumental record is used to determine annually averaged weather data extending from 1900 to 1998 A.D. The average annual surface temperature calculated for this period is 6.5 °C with a seasonal range of approximately 34 °C. The average annual precipitation for the same period is 815 mm with 60% of the rainfall occurring from May to September. A portion of this rainfall constitutes extreme rain events, which are characterized by greater than 3 in. (76 mm) of rain falling within a 24-hour period (Winkler, 1988).

The stalagmites were collected from the passage labeled Straight Shot East in SVC-II (Fig. 1) in August 1998. This 915-meter long passage, approximately 1 m in width and 2 m in height, is located at a depth of 21 m below the land surface. The stalagmites, SVC983-1 and SVC983-2, were joined at the base and grew from the floor of the passage. A third stalagmite, SVC982, was collected from a wall of the same cave room. SVC982, and SVC983-1 with lengths of 36.5 cm and 60.2 cm, respectively, were growing with active drips from the ceiling during the time of their collection. SVC983-2 is 35.7 cm long and stopped growing ~4600 yr B.P. (before 1950 A.D.). The samples were cut in longitudinal halves and polished. One half was archived and all analytical work was performed on the other half.

3. Analytical methods

3.1. ^{230}Th dating

The ages of stalagmite layers were determined by ^{230}Th dating, using U and Th separation techniques as outlined in Edwards et al. (1987) and Shen et al. (2003). We measured isotopic ratios on an inductively coupled plasma mass spectrometer (Finnigan Element I) adopting procedures from Shen et al. (2002). For ^{230}Th dating, subsamples were drilled at depth intervals of 4–282 mm for SVC983-1 and 10-70.5 mm for SVC982.

3.2. Fluorescence imaging

We imaged stalagmites using a BioRad MRC 1024 laser scanning confocal microscope fitted with a Kr/Ar laser source. The excitation

Table 1
Uranium and Thorium isotopic composition and ^{230}Th ages for stalagmites SVC983-1 and SVC982 from Spring Valley Caverns. Errors are 2σ of the mean.

Sample number	Depth[a] (mm)	^{238}U (ppb)	^{232}Th (ppt)	δ^{234}U[b] (measured)	[^{230}Th/^{238}U][c] (activity)	^{230}Th/^{232}Th[d] (ppm)	^{230}Th age (uncorrected) in years	^{230}Th age[c,e] (corrected)	^{230}Th age[f] in years B. P.	δ^{234}U[g] (initial)
SVC983-1										
SV98C24	4	2400±6	3086±110	654±3	0.00153±0.00011	19.7±1.5	100±7	80±13	27±13	654±3
SV98C25	7	3590±8	6000±105	616±2	0.00208±0.00010	20.6±1.0	140±7	113±15	60±15	616±2
SV98C30	11	2210±5	12955±120	632±2	0.00316±0.00018	8.9±0.5	210±12	116±49	62±49	632±2
D-11	11	2325±7	63450±40	630±4	0.00257±0.00026	15.5±1.6	170±17	128±28	72±28	630±4
SVC983-61	21	1333±4	78.2±1.3	634±4	0.00347±0.00015	978±46	230±10	230±10	180±10	634±4
SV98C09-1	31	3160±10	30±100	646±4	0.00466±0.00011	7335±21600	310±7	310±8	257±8	646±4
SV98C09-2	31	2890±6	90±50	642±2	0.00456±0.00009	2530±1390	304±6	303±6	248±6	642±2
SV98C06	70	1470±6	810±95	624±4	0.00832±0.00020	250±30	560±10	550±14	500±10	625±4
SV98C28	98	3050±9	1140±90	609±4	0.01042±0.00024	460±38	710±20	700±20	650±20	610±4
SV98C31	105	1100±3	100±170	613±2	0.01085±0.00041	2010±3450	740±30	735±30	680±30	615±2
SV98C32	112	2470±5	2974±95	604±2	0.01208±0.00019	165±6	825±10	805±16	750±20	605±2
SV98C33	120	2875±5	330±90	561±2	0.01216±0.00019	1770±510	850±10	850±10	800±10	562±2
SV98C10	128	2925±6	4040±120	581±3	0.01378±0.00023	165±6	955±20	930±20	880±20	583±3
SV98C38	138	2770±6	5055±100	573±2	0.01533±0.00039	140±4	1070±27	1040±30	980±30	575±2
SVC983-1-63	151.5	2350±7	2523±9	592±3	0.01550±0.00019	238±3	1070±10	1050±16	990±20	594±3
SV98C40	152	2430±5	1480±46	585±2	0.01535±0.00016	417±14	1060±10	1050±10	1000±10	586±2
SVC983-1-64	154	2186±6	1480±6	599±3	0.01573±0.00019	383±5	1080±10	1070±14	1010±10	600±3
SVC983-1-65	156	2050±6	602±2	578±3	0.01569±0.00012	880±7	1090±9	1090±9	1030±9	580±3
SVC983-1-66	168	2140±7	186.0±1.5	574±3	0.01684±0.00014	3207±36	1170±10	1170±10	1120±10	576±3
SVC983-1-67	177	2230±5	1550±4	560±2	0.01772±0.00014	421±3	1250±10	1230±10	1180±10	562±2
SV98C36	189	2520±5	2740±90	562±2	0.02059±0.00027	310±10	1450±20	1430±20	1370±20	564±2
SV98C12-1	206	2760±7	225±100	645±3	0.02305±0.00029	4670±2050	1540±20	1540±20	1490±20	647±3
SV98C12-2	206	2510±5	545±60	648±2	0.02297±0.00020	1745±190	1530±14	1530±14	1470±10	650±2
SV98C13	231	3150±8	14650±120	563±3	0.02480±0.000380	88.1±1.5	1740±30	1670±50	1610±50	566±3
SV98C41-1	250	2650±6	210±45	558±2	0.02651±0.00025	6290±2310	1870±20	1870±20	1820±20	560±2
SV98C41-2	250	2640±6	230±60	561±2	0.02658±0.00024	5010±1260	1870±20	1870±20	1820±20	564±2
SV98C14	256	2660±6	7360±90	571±2	0.02779±0.00029	166±3	1950±20	1900±30	1850±30	574±2
SV98C15	283	2630±5	1270±96	585±2	0.03173±0.00029	1080±80	2205±20	2200±20	2140±20	589±2
SV983-55	301	2700±8	2380±50	574±3	0.03452±0.00032	647±15	2420±23	2404±25	2350±25	578±3
SV98C17	341	1480±3	9660±108	793±3	0.04624±0.00073	117±2	2847±46	2751±66	2700±70	799±3
SV98CR1	350	930±2	554±90	777±3	0.04665±0.00041	1290±220	2900±26	2891±27	2840±30	783±3
SV98C04	382	1100±3	4878±90	685±4	0.04972±0.00062	186±4	3263±42	3194±55	3140±55	692±4
SVC982										
SV982-2	10	2013±5	1674±12	771±3	0.00070±0.00030	3.52±0.51	60±16	45±16	-3±16	771±3
SV982-5	13.5	972±3	3306±60	730±4	0.00273±0.00024	13.2±1.8	170±15	120±30	60±30	730±4
SV982-19	28	1400±7	86.4±1.4	718±6	0.00443±0.00013	1190±40	280±9	280±9	225±9	719±6
SVC982-17	44.5	955±3	108.0±1.3	769±4	0.00602±0.00022	880±34	370±14	370±14	310±14	769±4
SV982-4	70.5	1708±5	2034±47	696±3	0.00961±0.00017	133±4	620±10	610±10	550±14	697±3
SVC982-16	70.5	1120±4	2044±13	698±3	0.01004±0.00028	90±3	650±20	620±20	560±20	699±3

[a] Distance of the midpoint of the drill hole from top of the stalagmite.
[b] $\delta^{234}U = ([^{234}U/^{238}U]\text{activity} - 1) \times 1000$.
[c] $[^{230}Th/^{238}U]\text{activity} = 1 - e^{-\lambda 230 T} + (\delta^{234}U_{\text{measured}}/1000)[\lambda_{230}/(\lambda_{230} - \lambda_{234})](1 - e^{-(\lambda 230 - \lambda 234)T})$, where T is the age. Decay constants are 9.1577×10^{-6} yr^{-1} for ^{230}Th, 2.8263×10^{-6} yr^{-1} for ^{234}U (Cheng et al., 2000), and 1.55125×10^{-10} yr^{-1} for ^{238}U (Jaffey et al., 1971).
[d] The degree of detrital ^{230}Th contamination is indicated by the [^{230}Th/^{232}Th] atomic ratio instead of the activity ratio.
[e] Age corrections were calculated using ^{230}Th/^{232}Th atomic ratio of $4.0 \times 10^{-6} \pm 2.0 \times 10^{-6}$. The errors are arbitrarily assumed to be 50%.
[f] Corrected ages reported as yr B.P. where P = 1950 A.D.
[g] δ^{234}Uinitial corrected was calculated based on ^{230}Th age (T), i.e., $\delta^{234}U_{\text{initial}} = \delta^{234}U_{\text{measured}} \times e^{\lambda 234 * T}$, and T is corrected age.

and emission wavelengths used were 488 nm and 522 nm, respectively. Fluorescent bands were detected and counted from these digital images. Counting bands three to five times provided a mean and a standard deviation of the band counts. The fluorescent scan of SVC983-1 extends from the top (0 mm) to ~380 mm depth corresponding to an age of ~3000 yr B.P. and the scan of SVC982 extends from top to ~60 mm, representing an age of ~650 yr B.P.

3.3. Hydrological modeling

To determine the relationship between the nature of rainfall events and cave flooding, we constructed a simple hydrologic model. The complexities involved in modeling a real cave system currently preclude explicit simulation of the system in all its detail. Instead, we considered a basic hydrologic cave model (Fig. 2) with parameters estimated from field studies and topographic maps. The primary objective of this model was to perform a comparative study of flood height and duration in the cave caused by both extreme and average rainfall events.

In this model all types of fluxes into the cave are combined to one volumetric influx parameter, $Q_{in}^t = \phi P^t A_w$, at time step t, where P^t is the precipitation rate (m/day) that occurred over the watershed area, A_w, and ϕ is the fraction of the total water flux from the watershed that actually enters the cave. Over a time interval, Δt, i.e., during time step t, the water level in the cave rises by $h^t = Q_{in}^t \Delta t / A_c$, where A_c is the floor area of the cave, assumed to be a tank with perfectly vertical walls and negligible volume reduction by stalagmites, stalactites, and other protrusions. Any influx into the cave at time t is added to the water level from the previous time step, h^{t-1}, minus the outflux, Q_{out}^{t-1}, that occurs during the previous time step, assuming that all water is added instantaneously at the beginning of the time step and then allowed to drain over the time step interval, Δt. Setting the arbitrary reference elevation, z, for water level (i.e., the elevation head component of the hydraulic head) measurements to zero at the cave outflow position and, assuming laminar flow within a narrow, low-hydraulic-conductivity outlet allowing approximation of outflow conditions by Darcy's law for simplicity, the outflux from the cave is given as $Q_{out}^{t-1} = KA_o h^{t-1}/\Delta x$, during the previous time step, $t-1$, where K, A_0, and Δx are the hydraulic conductivity (in m/s), the cross-sectional area of the outlet, and the length of the cave's conceptual water outlet, respectively. In our model a linear relationship is assumed between the outflux, Q_{out}^{t-1}, and hydraulic head gradient, $h^{t-1}/\Delta x$, because as Δt is short there is negligible reductions in hydraulic head, h^{t-1}, within Δt. The reduction in water level in the cave over Δt during the previous time step is then given as $h_{out}^{t-1} = Q_{out}^{t-1}\Delta t / A_c$. In summary, the water level height (i.e., hydraulic head), h, in the cave at time t is

$$h^t = h_{in}^t + h^{t-1} - h_{out}^{t-1} = \phi \frac{A_w}{A_c}\Delta t P^t + \left(1 - \frac{(A_o K)\Delta t}{A_c \Delta x}\right) h^{t-1}. \quad (1)$$

In this model, a flood occurs when the water level height, h, exceeds some minimum water level height, h_{min}, which is one of the main model calibration parameters. To estimate the watershed area A_w, the USGS topographic sheet for Spring Valley, MN (N4337.5–W9222.5/7.5) was used. The cave area, A_c, was determined as a percentage of the watershed area from the map. As the cross-sectional area, A_0, the length, Δx, and the hydraulic conductivity, K, of the outlet cannot be estimated independently, the combined term $A_0K/\Delta x$ in Eq. (1), is used as one of three main calibration parameters during the calibration phase of the model (i.e., transfer function) development, covering the period 1950–1998. The other main calibration parameters are h_{min} and ϕ. As A_w and A_c are at least somewhat constrained by measurements, as described above, variations of their values are kept to a minimum during the calibration phase of the model. P is the forcing input parameter to the model. A code was prepared in MATLAB® to execute the model.

4. Results

4.1. ^{230}Th dates

High concentrations of ^{238}U of 1–3 ppm were measured in the Spring Valley stalagmites, allowing precise dating by the ^{230}Th method. Twenty-eight ^{230}Th dates for sample SVC983-1 (including 4 replicates) and 5 dates (including 1 replicate) for SVC982 are listed in Table 1. The 2σ ^{230}Th dating precision ranges from ±6 to 30 yr for most subsamples of SVC983-1. Only 4 subsamples were ^{230}Th dated with error >30 yr due to high detrital thorium contents of 10–15 ppb. Six subsamples of SVC982 were dated with precision of ±9–30 yr.

4.2. Fluorescent image

Each fluorescent band consists of a couplet of a fluorescing lighter and a non-fluorescing darker part (Fig. 3), varying in width between

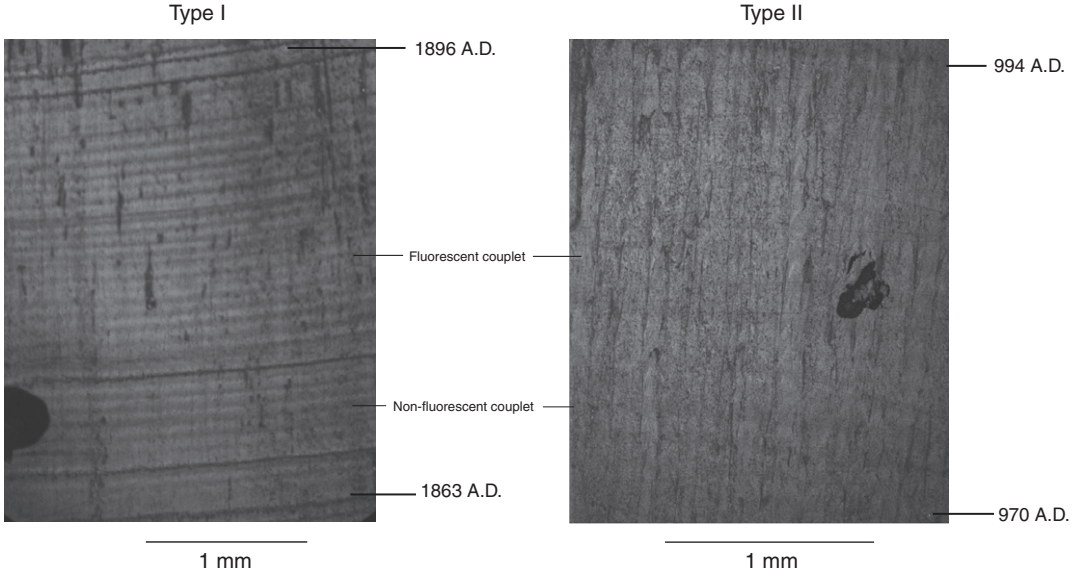

Fig. 3. Type I (left) and Type II (right) fluorescent banding. Type I banding shows organic-rich, light-colored fluorescent bands and organic-poor, darker, non-fluorescent bands. These darker bands are not clearly visible in Type II banding.

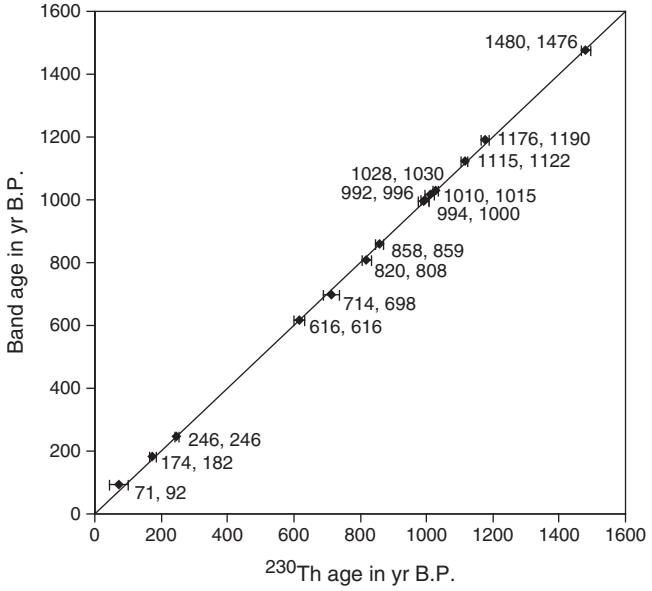

Fig. 4. Plot of band counted age against ^{230}Th age. The diagonal line marks 1:1 relationship between the band age and the ^{230}Th age and is not a regression line. The numbers next to each data point denote the ^{230}Th age and band age, respectively. All ages are reported as years B.P. The band ages are constrained by the ^{230}Th age of 246 ± 6 yr.

10 and 200 μm. Based on their characteristics the banding is divided into two types. Type I banding exhibits a clear distinction between the light and the dark parts with an average ratio of 1.3. The Type II bands are characterized by either very closely spaced lighter bands and thin to almost non-existent darker bands or lesser intensity variation between the light and the dark parts. The average width ratio of light to dark part is 2.5 for Type II banding.

To test if the bands represent annual deposition, we compare the number of bands between consecutive ^{230}Th ages with the difference of those ages. A section from 3 to 15 cm depth is chosen from SVC983-1, spanning approximately 1000 yr. We select precise ^{230}Th dates that have very little detrital correction to count bands between consecutive dates. Comparison of band numbers with age differences shows that the Type I band count matches well with the age difference and that the error in band count is approximately 6%. In contrast, the Type II band count falls short of the ^{230}Th age by an average of 55%. We construct an absolute chronology for the samples using the combined method of band counting and ^{230}Th dating as discussed in Dasgupta (2008) and illustrated in Fig. 4. This combined method is applied up to 1500 yr B.P. Beyond this age, the banding is too ambiguous to be used and hence we use linear interpolation between ^{230}Th dates to construct the chronology past 1500 yr B.P.

4.3. Flood bands

In addition to the couplets of fluorescent and non-fluorescent bands, another type of non-fluorescing dark banding was observed in the samples. These dark bands appear opaque under an optical microscope (Fig. 5). Electron microprobe analysis of these opaque layers identified them as detrital components possibly comprising mixtures of ilmenite, plagioclase, quartz, and clay minerals. We interpret these detrital layers as being caused by floods that deposited the detrital components on top of the stalagmites. Hence, we term the detrital layers "flood bands" hereafter.

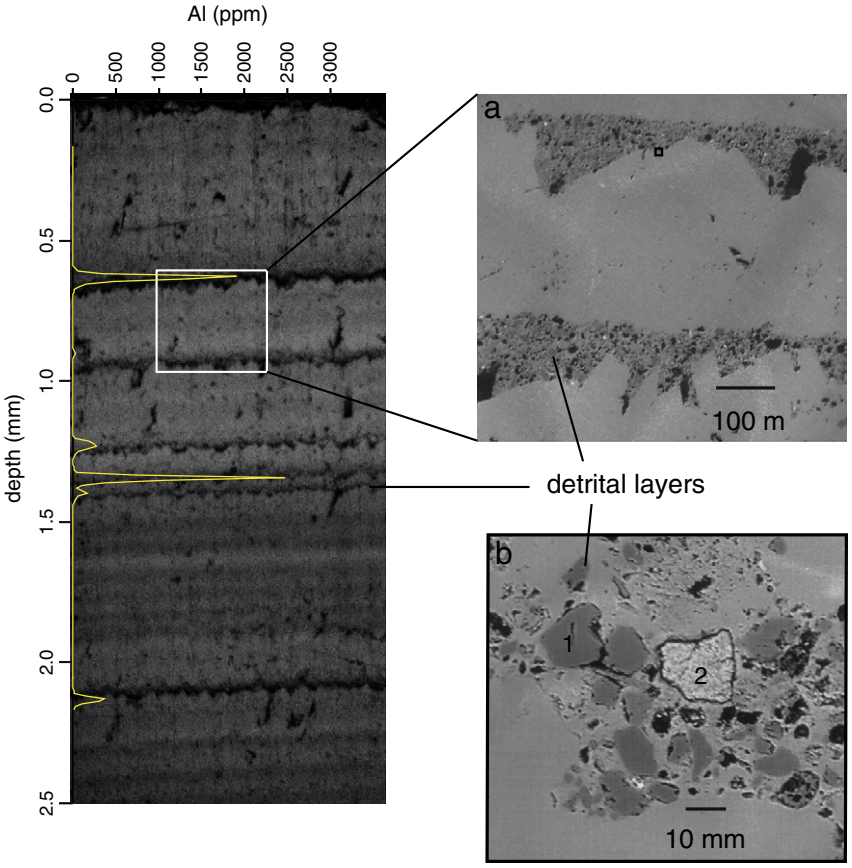

Fig. 5. Confocal micrograph on the left, showing flood bands or detrital layers from SVC982 from 1973 A.D. at the base to 1998 A.D. at the top. A plot of Al concentration is superimposed on the graph showing Al peaks coinciding with detrital layers. The panels on the right show details of each detrital band. In panel (a) the structure of the dark detrital layers are shown; the lighter phase between the two layers is calcite. The phases in (b) are quartz (1) and an iron-rich phase (2).

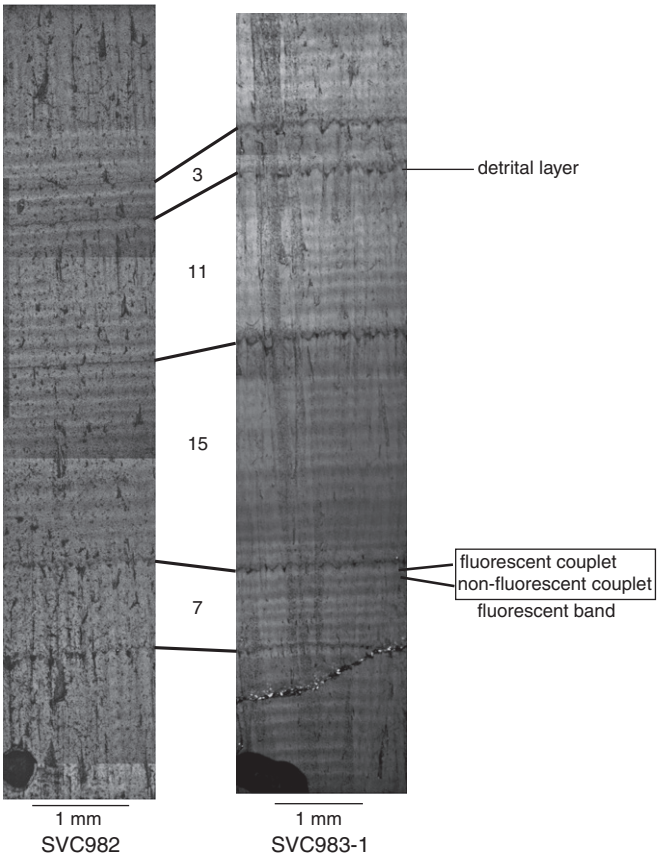

Fig. 6. Confocal micrographs of SVC982 and SVC983-1. The tie-lines connect coeval flood bands and the numbers between them denote number of fluorescent bands. The two sections span 54 yr from 1656 A.D. at the base to 1710 A.D. at the top.

We compare the number of flood bands between samples SVC982 and SVC983-1 over contemporaneous growth periods and observe excellent replication of the flood band patterns in the two samples (Fig. 6). While the thickness of individual fluorescent bands varies, two consecutive flood bands are always separated by a comparable number of fluorescent bands, consistent with identical timing of flood band formation. This replication of band patterns in the two samples demonstrates their importance as proxies for past cave floods and as chronological tools.

4.4. Model results

The model results yield height of water in the cave after each rainfall event as given in the instrumental record. The resolution of flooding recorded in stalagmite bands being yearly, the temporal resolution of modeled water level heights in the cave h^t, is subsequently reduced to yearly time steps so that one or more modeled floods in a year are grouped together, and that year is denoted a "flood year" (given a value of one). Years without any modeled floods are denoted non-flood years (given a value of zero). These results are then directly compared to the actual record of flood bands in stalagmites to provide a measure of accuracy of the model. As the number of observed flood years is less than the number of non-flood years, a weighting factor is designed such that 50% accuracy is obtained for the cases of i) correct prediction of all non-flood years but incorrect prediction of all flood years and ii) correct prediction of flood years but incorrect prediction of all non-flood years. During the calibration phase (1950–1998) of model development, parameters $KA_o/\Delta x$, h_{min}, ϕ, and to some degree A_w, A_c, (see Section 3.3) are explored in parameter space by varying their values iteratively, minimizing the misfit between observed and modeled flooding events. The model is then verified with the instrumental record of rainfall from 1900–1949 resulting in an accuracy of 72%, with correct predictions of 4 flood years and 29 non-flood years (Fig. 7). The model results in a greater likelihood of cave flooding from an extreme event than from an event with a large total precipitation that is distributed over a longer time interval.

5. Discussion

Our analysis of the fluorescent banding shows that these bands represent an annual record with an uncertainty of approximately 6%. Both the detrital nature of the flood bands, as established from microprobe analysis (Section 4.3), and the model results (Section 4.4), reasonably reproducing flood events and non-flooding periods in the cave, suggest that these layers are indicators of cave floods due to

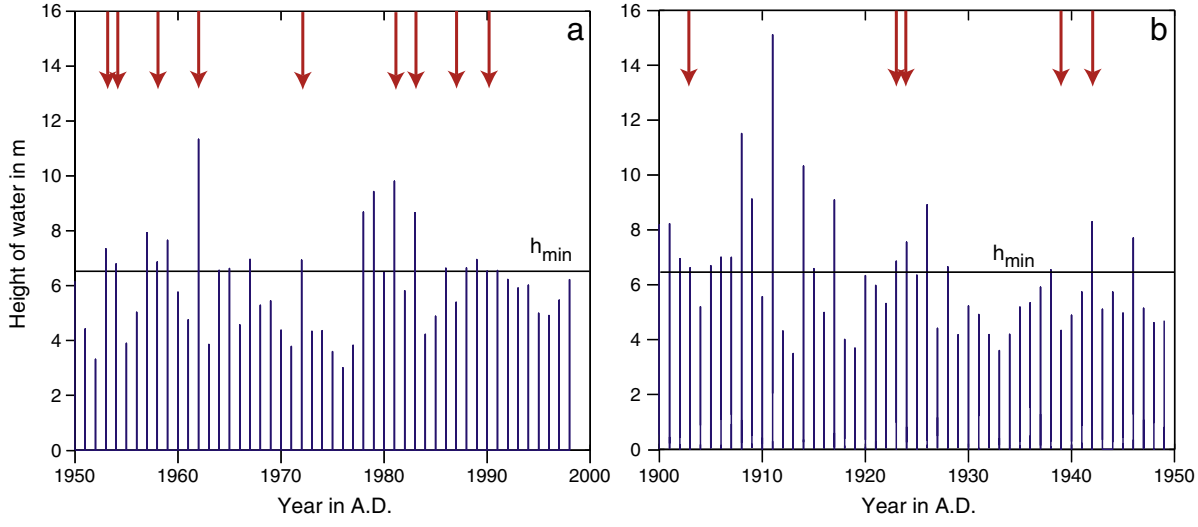

Fig. 7. Results from numerical model runs showing flooding in the cave represented by water height in meters. a) Results for the calibration period (1950–1998 A.D.). b) Results for the verification period (1900–1949 A.D.). The horizontal bar represents the cut off height of flood water in the cave as described in Section 3.3. The red arrows at the top are flood years as observed in the samples.

extreme rainfall events. To investigate the variability of these events through time, we construct a time series of cave-flood frequency, henceforth termed flood frequency, for the past three thousand years. Flood frequency reconstructions for samples SVC982 and SVC983-1 cover the time periods 1340–1998 A.D. and 900 B.C.–1920 A.D., respectively, showing good agreement for the overlapping time segment (1340–1920 A.D.) (Fig. 8). Thus, we combine the data sets of both time periods to a composite flood frequency time series (Fig. 9).

5.1. Cave-flood frequency analysis

For the total 3000-yr period, the average frequency of flood occurrences, and hence inferred extreme rainfall events, per century is 5. The number of extreme events per century shows a significant increase during the 19th and 20th centuries with 13 events occurring during the last 100 yr. Previously, only the 3rd and 5th centuries A.D. recorded 10 and 11 events, respectively. At a temporal resolution of 50 yr, the flood frequency suggests an increase in extreme rainfall events during the latter half of the 19th century. At a yet higher temporal resolution of decades, we observe that decades experiencing 3 or more extreme rainfall events include 641–650 and 571–580 B.C. as well as 240–249, 1280–1289, 1860–1869, 1850–1859, and 1980–1989 A.D. Of these, 240–249 A.D. had 5 and 1980–1989 A.D. had 4 extreme rainfall events. Conversely, the 3rd century B.C. recorded no extreme event and the 8th century B.C. and the 6th and 14th centuries A.D. recorded only 1 extreme event each.

To test the possible link between these extreme events and past hydrological conditions, we calculate a cave-flood index (henceforth termed flood index) from the Spring Valley Caverns flood record by subtracting the mean number of events per century (calculated for the last 3000 yr) from the observed number of events in a given century and then dividing that value by the standard deviation. This results in an index that represents the number of standard deviations above (positive) or below (negative) the centennial mean flood frequency (Fig. 10). Positive values of this index suggest intervals with the most extreme events while negative values represent below average to non-occurrence of extreme rainfalls. We compare this flood index with the paleohydrological record reconstructed by Booth and Jackson (2003) from testate amoeba analysis from a peat bog in Michigan. Booth et al. (2006) have also shown a correlation between hydrological records from north-central Minnesota and southeastern Michigan during times of high moisture fluctuation. Even though there is not an exact peak-to-peak match between the flood index and the composite paleohydrological index, a broader correlation can be observed (Fig. 10) between higher values of the flood index with higher values of paleohydrological index, implying more occurrences of extreme rainfall events during higher moisture availability. Notably, both of the records show increased values since the 20th century.

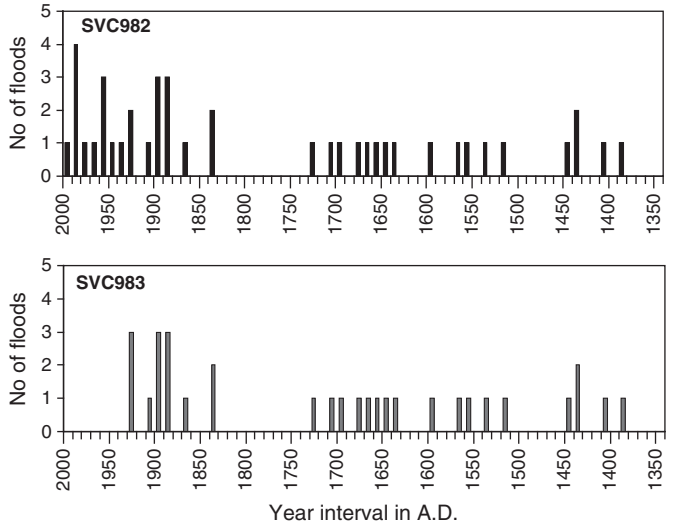

Fig. 8. Comparison of decadal flood frequency from SVC983 and SVC982 for the overlapping period of record from 1340 to 1920 A.D.

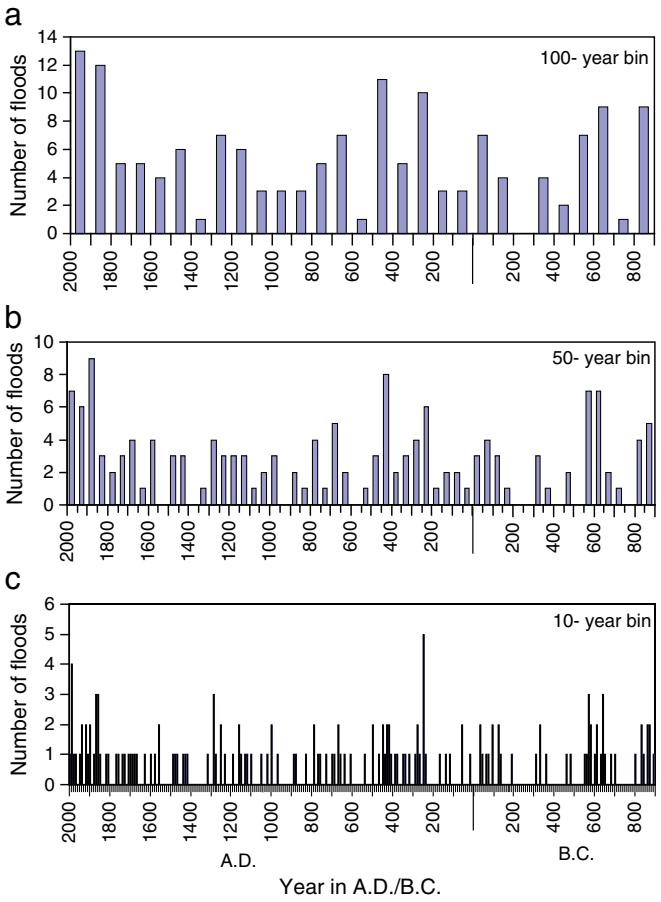

Fig. 9. Plots showing number of floods per 100 yr (a), per 50 yr (b), and per decade (c).

5.2. Land use pattern and cave flooding

The increase in flood frequency since about 1850 A.D. can likely be attributed to climatic changes or changes in land use pattern or to a complex interaction of both. After the settlement of European farmers in ~1850 A.D., the landscape changed from prairie–savannah to farmlands. Agricultural practices underwent several changes during the last 160 yr involving changes in the type of crops, which in turn affected land use and soil erosion. This landscape change led to increased soil erosion and run-off and one could argue, might have increased cave flooding.

A close analysis of the flood frequency data shows an increase in flood frequency since the second half of the 19th century. The 50-yr flood frequency data shows 9 events in the interval 1850–1899 A.D., followed by a decrease to 6 events in 1900–1949 A.D and then 7 events in 1950 to 1998 A.D. At a shorter time-scale, each of the decades 1850–1859 and 1860–1869 A.D. experienced 3 flooding events, and the decade 1980–1989 A.D. experienced 4. Weather records indicate that 1850 to 1915 was a wet period, 1915 to 1960 was dryer than average, including the dust-bowl drought of the 1930s, and the last three decades of the 20th century have been wetter than

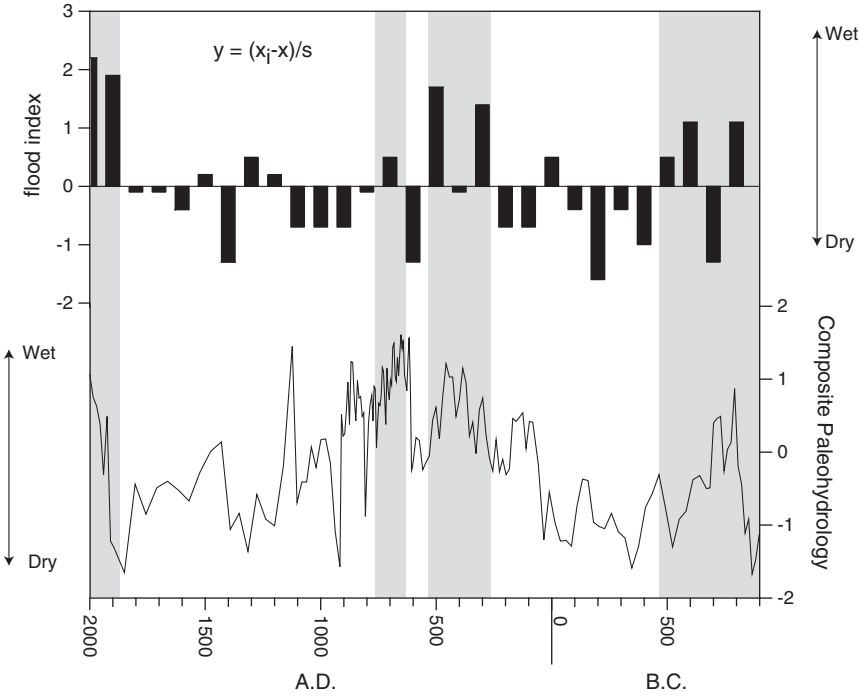

Fig. 10. Comparison of flood frequency index with past moisture variability reconstructed from a raised bog in Michigan (Booth and Jackson, 2003). The vertical bars demarcate intervals of wetter conditions in Michigan and more cave floods in Spring Valley Caverns.

average. The cave-flood frequency closely follows this trend. Further, this type of extreme flood frequency is not completely unprecedented before the arrival of the European settlers as 7 flooding events occurred in the interval 650–601 B.C., followed by an additional 7 events in 600–551 B.C. Therefore, it is likely that climate played the dominant role in the occurrence of flooding within Spring Valley Caverns.

6. Conclusion

Confocal fluorescence microscopy allowed the identification and imaging of detrital layers in stalagmites from Spring Valley Caverns (SVC). Combination of high-resolution ^{230}Th dating and annual fluorescent band counting provided a high-resolution chronology to these layers. Comparative study with instrumental data and modeling work strongly suggested that these detrital layers originated from short lived extreme rain events, such as thunderstorms, establishing that detrital layers in cave calcite could be potential proxies of past extreme rainfall events. The SVC record shows that the frequency of these extreme events has undergone changes in the last 3000 yr with the most increase in these events occurring during the latter part of the twentieth century. This 20th century increase in flood frequency also coincides with the rise in mean annual surface temperature. Comparison with regional records of paleohydrology shows an increase in the incidence of these events during times of higher moisture availability. Moreover, a simulation of 21st century water balance change in the Great Lakes region suggests increased moisture transport in this region due to global warming (Kutzbach et al., 2005). Combined with our observation of increased flood frequency during increased moisture content in the past, these models suggest a greater incidence of extreme rainfall events in Minnesota in the future under global warming conditions.

Acknowledgment

This work was supported by Gary Comer Science and Education Foundation Grant CC8, National Science Foundation Grant EAR-0902867, GSA Research Fellowship, University of Minnesota Dennis and Emmons Fellowship. This work was also partially supported by NSF grant No. EAR-0941666 and by funds from George and Orpha Gibson for the Hydrogeology and Geofluids Research Group. We thank John Ackerman, the owner of Spring Valley Caverns, for donating the stalagmites to E. Calvin Alexander, Jr. for scientific study and his continued support of research in Spring Valley Caverns. Scott Alexander's valuable and insightful inputs are greatly acknowledged. We gratefully acknowledge Luis Gonzalez for sharing his methodology of confocal laser microscopy. S.D. thanks Shameek Bose for help with Matlab codes. Finally, we thank the two anonymous reviewers for their insightful comments that helped to improve the manuscript.

References

Baker, A., Smart, P.L., Edwards, R.L., Richards, D.A., 1993. Annual growth banding in a cave stalagmite. Nature 364, 518–520.

Baker, A., Genty, D., Smart, P.L., 1998. High-resolution records of soil humification and paleoclimate change from variations in speleothem luminescence excitation and emission wavelengths. Geology 26, 903–906.

Booth, R.K., Jackson, S.T., 2003. A high-resolution record of late-Holocene moisture variability from a Michigan raised bog, USA. The Holocene 13, 863–876.

Booth, R.K., Notaro, M., Jackson, S.T., Kutzbach, J.E., 2006. Widespread drought episodes in the western Great Lakes region during the past 2000 years: geographic extents and potential mechanisms. Earth and Planetary Science Letters 242, 415–427.

Cheng, H., Edwards, R.L., Hoff, J., Gallup, C.D., Richards, D.A., Asmerom, Y., 2000. The half-lives of uranium-234 and thorium-230. Chemical Geology 169, 17–33.

Dasgupta, S., 2008. High-resolution speleothem record of late Quaternary climate change from the Upper Midwest. University of Minnesota, USA.

Dorale, J.A., Lepley, S.W., Edwards, R.L., 2005. The ultimate flood recorder: flood-deposited sediments preserved in stalagmites. European Geosciences Union, Vienna, Austria.

Edwards, R.L., Cheng, J.H., Wasserburg, G.J., 1987. ^{238}U–^{234}U-^{230}Th-^{232}Th systematics and the precise measurement of time over the past 500,000 years. Earth and Planetary Science Letters 81, 175–192.

Frappier, A.B., Sahagian, D., Carpenter, S.J., González, L.A., Frappier, B.R., 2007. Stalagmite stable isotope record of recent tropical cyclone events. Geology 35, 111–114.

Jaffey, A.H., Flynn, K.F., Glendenin, L.E., Bentley, W.C., Essling, A.M., 1971. Precision measurement of half-lives and specific activities of U-235 and U-238. Physical Reviews 4, 1889–1906.

Karl, T.R., Knight, R.W., Plummer, N., 1995. Trends in high-frequency climate variability in the twentieth century. Nature 377, 217–220.

Kunkel, K.E., Andsager, K., 1999. Long-term trends in extreme precipitation events over the coterminous United States and Canada. Journal of Climate 12, 2515–2527.
Kutzbach, J.E., Williams, J.W., Vavrus, S.J., 2005. Simulated 21st century changes in regional water balance of the Great Lakes region and links to changes in global temperature and poleward moisture transport. Geophysical Research Letters 32, L17707.
Nyberg, J., Malmgren, B.r.A., Winter, A., Jury, M.R., Kilbourne, K.H., Quinn, T.M., 2007. Low Atlantic hurricane activity in the 1970s and 1980s compared to the past 270 years. Nature 447, 698–702.
Polyak, V.J., Asmerom, Y., 2001. Late Holocene climate and cultural changes in the Southwestern United States. Science 294, 148–151.
Schumacher, R.S., Johnson, R.H., 2006. Characteristics of U.S. Extreme Rain Events during 1999–2003. Weather and Forecasting 21, 69–85.
Shen, C.-C., Edwards, R.L., Cheng, H., Dorale, J.A., Thomas, R.B., Moran, S.B., Weinstein, S.E., Edmonds, H.N., 2002. Uranium and thorium isotopic and concentration measurements by magnetic sector inductively coupled plasma mass spectrometry. Chemical Geology 185, 165–178.
Shen, C.-C., Cheng, H., Edwards, R.L., Moran, S.B., Edmonds, H.N., Hoff, J.A., Thomas, R.B., 2003. Measurement of attogram quantities of ^{231}Pa in dissolved and particulate fractions of seawater by isotope dilution thermal ionization mass spectroscopy. Analytical Chemistry 75, 1075–1079.
Winkler, J.A., 1988. Climatological characteristics of summertime extreme rainstorms in Minnesota. Annals of the Association of American Geographers 78, 57–73.
Yiou, P., Nogaj, M., 2004. Extreme climatic events and weather regimes over the North Atlantic: when and where? Geophysical Research Letters 31, L07202. doi:07210.01029/02003GL019119.